Available online at www.sciencedirect.com
ScienceDirect
International Journal of Heat and Mass Transfer 51 (2008) 3091–3102
International Journal of HEAT and MASS TRANSFER
www.elsevier.com/locate/ijhmt

Combined heat and mass transfer for laminar flow of moist air in a 3D rectangular duct: CFD simulation and validation with experimental data

Prabal Talukdar [a,*], Conrad R. Iskra [b], Carey J. Simonson [b]

[a] Department of Mechanical Engineering, Indian Institute of Technology Delhi, New Delhi 110 016, India
[b] Department of Mechanical Engineering, University of Saskatchewan, 57 Campus Drive, Saskatoon, SK, Canada S7N 5A9

Received 20 April 2007; received in revised form 10 August 2007
Available online 14 November 2007

Abstract

Computational fluid dynamics (CFD) simulations are performed for convective heat and mass transfer between water surface and humid air flowing in a horizontal 3D rectangular duct. A hydrodynamically fully developed flow of moist air flows over the surface of a water tray. As the air flows over the water tray, water evaporates from water tray to the air stream. Evaporation cools the water until sensible heat transfer from the air equals the latent heat of evaporation. As the water temperature decreases below the air temperature, a simultaneous heat and mass transfer process with heat and mass transfer in opposite direction occurs. This phenomenon was studied experimentally in a previous work and has already been reported. In the present work, attempt has been done to model the same experiment. Numerical and experimental data are compared and sensitivity studies are carried out to understand the discrepancies between them. Effect of Rayleigh number is found to be negligible. Effect of introducing a heat source/sink at the water surface could result negative Nusselt and Sherwood number. Heat and mass transfer analogy is defined for a combined heat and mass transfer problem.

Keywords: Heat and mass transfer; Natural convection; Mixed convection; Nusselt number; Sherwood number; 3D; Laminar flow

1. Introduction

In nature and many industrial applications, there are plenty of transport processes where simultaneous heat and mass transfer is a common phenomenon. Its application is found in many diverse fields but not limited to cleaning operations, curing of plastics, manufacturing of pulp-insulated cables, many chemical processes, building sciences [1–3], food processes [4], condensation and frosting of heat exchangers [5–7], moisture transfer between flowing air and porous media [8] and atmospheric flows. The study of convection reduces to the determination of convective heat and mass transfer coefficients. Convective heat and mass transfer coefficients are important parameters, which are a measure of the resistance to heat and mass transfer between a surface and the fluid flowing over that surface. The convective coefficients depend on the hydrodynamic, thermal and concentration boundary layers. In many of the internal flows, both forced and natural convection play major roles in the heat and mass transfer processes. Whereas in the entrance section of a duct, forced convection becomes dominant, as the flow moves towards the downstream section, natural convection could dominate over forced convection and finally in the thermally developed region natural convection becomes negligible. Natural convection may be due to a temperature or concentration gradient or both. If the buoyancy forces are due to temperature and concentration gradients that act in the same direction, both the heat and mass transfer will increase. However, if the temperature and concentration gradients act in the opposite direction, both heat and mass transfer reduce.

* Corresponding author. Tel.: +91 11 2659 6337; fax: +91 11 2658 2053.
E-mail address: prabal@mech.iitd.ac.in (P. Talukdar).

0017-9310/$ - see front matter © 2007 Elsevier Ltd. All rights reserved.
doi:10.1016/j.ijheatmasstransfer.2007.08.034

Nomenclature

b	width of water pan (m)
C	vapor density or vapor concentration of air (kg/m^3)
Cp	specific heat capacity at constant pressure (J/(kg K))
D_{AB}	binary vapor diffusion coefficient (m^2/s)
D_h	hydraulic diameter (m)
g	gravitational acceleration (m/s^2)
h	convective heat transfer coefficient (W/(m^2 K))
h_{fg}	latent heat of vaporization (J/kg)
h_m	convective mass transfer coefficient (m/s)
H	height of the duct (m)
k	thermal conductivity of air (W/(m K))
L	length of the duct (m)
m	index
n	normal to the wall, index
MW_a	molecular weight of air (kg/mol)
MW_v	molecular weight of water vapor (kg/mol)
Nu	Nusselt number ($=hD_h/k$)
P	Pressure (Pa)
Pr	Prandtl number ($=\nu/\alpha$)
Ra	Rayleigh number $=\left(\frac{g\beta(T_w-T_0)\rho^2 C_p D_h^3}{\mu k}\right)$
Re	Reynolds number based on hydraulic diameter ($=\rho w_{av} D_h/\mu$)
RH	relative humidity
S^*	dimensionless parameter that represents the ratio between mass and heat transfer
Sc	Schmidt number ($=\nu/D_{AB}$)
Sh	Sherwood number ($=h_m D_h/D_{AB}$)
T	temperature (K) or if specified (°C)
u, v, w	velocity component in x, y and z directions (m/s)
W	width of the duct (m)
x,y,z	coordinate directions/length (m)

Greek symbols

α	thermal diffusivity of air (m^2/s)
β	volumetric expansion coefficient for temperature (1/K)
β^*	species expansion coefficient (m^3/kg)
γ	aspect ratio ($=W/H$)
μ	dynamic viscosity of air (N s/m^2)
ν	kinematic viscosity of air (m^2/s)
ρ	density of air (kg/m^3)
ΔT, ΔC	log mean temperature, vapor density difference (°C), (kg/m^3)

Subscripts

av	average or mean
m	bulk mean
o	properties at the inlet of the test section ($z = 0$ m)
out	properties at the outlet of the test section ($z = 0.6$ m)
sat	saturated
w	properties at the water surface ($y = 0$)
z	local properties at position z (in the flow direction)

There are a lot of research works on the determination of heat and mass transfer coefficients considering the effect of buoyancy forces and a large share of it belongs to the internal flows [9–32]. Whereas some of the works consider only heat transfer [9–15,24–28] to quantify Nusselt number, many of them treat simultaneous heat and mass transfer [16–23,29,30] to determine Nusselt and Sherwood numbers together. Most of the works in the literature present numerical data and correlations [9–13,16–22,24–28,30] with only a few presenting experimental data and correlations [14,15,23,29]. Only the works which are most relevant to the present work will be discussed here.

1.1. Mixed convection with buoyancy effects due to thermal diffusion

Cheng and his co-workers studied mixed convective heat transfer for a fully developed flow in a horizontal rectangular duct with different limitations. In [9], results presented are applicable for long channels. Cheng et al. [10] discussed mixed convective heat transfer in the entrance region of a rectangular duct with the assumption of a large Prandtl number. They assumed constant heat flux at the walls with different aspect ratios and showed that the secondary velocity induced due to buoyancy force significantly enhances the heat transfer process and reduces the thermal entrance length. Without the restriction of large Prandtl number, there are detailed numerical studies of mixed convective heat transfer in the entrance region of a horizontal rectangular channel by Abou-Ellai and Morcos [24], Incropera and Schutt [25], Mahaney et al. [26], Lin and Chou [27] and Lin et al. [28].

1.2. Natural convection with buoyancy effects due to both thermal and mass diffusion

The nature of vertical natural convection flows resulting from the combined buoyancy effects of thermal and mass diffusion has been discussed by Gebhart and Pera [18]. They performed similarity solution technique to solve the set of equations and showed the advantages and applicability of the method compared to the then existing integral method. Natural convection with opposing buoyancy forces in a vertical channel was studied both experimentally and numerically by Lee and Parikh [29]. They pointed out the failure of similarity solution technique for a vertical

plate of finite length if flow reversal occurs and showed a better time dependent solution method which could handle such complexities.

1.3. Mixed convection with buoyancy effects due to both thermal and mass diffusion

In the recent years, Lin and his co-workers have contributed to the mixed convective heat transfer with combined buoyancy effects. Lin et al. [16] discussed the heat and mass transfer in a vertical pipe with wetted wall and found that the buoyancy forces have considerable effects on laminar forced convection. A study has also been carried out by Lin et al. [17] for heat and mass transfer in a horizontal square duct. A uniform temperature and uniform concentration was assumed at the bottom wall whereas other walls were kept at zero heat or mass flux. To investigate the onset of convective instability, similar studies were carried out by Lin and Tzeng [21] for flow of humid air in a 3D rectangular duct. They performed a numerical study considering buoyancy forces due to temperature and concentration gradients and latent heat transfer due to the vaporization of a liquid–water film. All the sides and the top wall of the duct were adiabatic and the bottom wall was a heated thin film of water at a constant temperature and concentration. They presented the effects of bottom wall temperature, air relative humidity, duct aspect ratio and Rayleigh number on the local Nusselt (Nu) and Sherwood number (Sh), but did not compare with experimental data.

Studies have been carried out by Yan and his co-workers for simultaneous heat and mass transfer in laminar mixed convection flows. Yan et al. [30] investigated flow between vertical parallel plates with asymmetric heating. Results are specifically presented for an air–water system under various heating conditions. In another work, Yan [20] used a numerical model to investigate thermal and concentration buoyancy effects on laminar mixed convection in horizontal rectangular ducts. Constant temperature and concentration boundary conditions were assumed on the four boundaries of the duct where a fluid entered with a specified temperature and concentration and a fully developed velocity profile. He presented a systematic study of the effect of Rayleigh number on Nu and Sh for different aspect ratios of the duct. He also presented the effect of buoyancy ratio (ratio of buoyancy force due to temperature gradient to concentration gradient) on Nu and Sh. Their results [20,30] were not compared with any experimental data.

1.4. Scope of the present work

Despite the large number of papers on convective heat and mass transfer, there are few papers that combine accurate experimental measurements and detailed numerical model. For the particular application of this paper, simultaneous heat and mass transfer in a short duct with buoyancy force due to both thermal and concentration differences [23], there appears to be no paper which compares both experimental and numerical data on convective mass transfer coefficients or Sherwood number. This paper will compare the experimental data of [23] and simulation results from CFD. This will verify the CFD model and experimental data. Contrary to the previous numerical work of Lin and Tzeng [21] which is the closest to the experimental test configuration of [23], a cold water surface is assumed to represent the bottom boundary of the rectangular enclosure in this paper instead of a hot water film as in [21]. In addition, the modeling of boundary condition at the water surface is done in a different way in this work. Instead of a constant temperature and concentration boundary condition [20,21], temperature and concentration at the water surface is calculated based on the fact that latent heat of evaporation is equal to the sensible heat transfer from air to water. In addition, heat and mass transfer analogy is defined with a new non-dimensionless parameter. While comparing the numerical and experimental data, various possibilities of the differences between the data sets are analyzed.

2. Problem description

Experiments are performed using the transient moisture transfer (TMT) facility at University of Saskatchewan. The experimental apparatus, procedure, uncertainty analyses and results are presented in the work of Iskra and Simonson [23] and hence will not be described here. The test section within the TMT is a horizontal rectangular duct, where heat and mass transfer occurs at the bottom wall surface. The facility passes air at varying velocities, temperatures and relative humidities above an open tray of water to determine the convective mass transfer coefficients.

In experiments, the convective mass transfer coefficient is determined for the horizontal rectangular duct by measuring (1) the evaporation rate from the rectangular tray of water that is located in the lower panel of the duct and (2) the vapor density difference between the air stream and the surface of the water. The vapor density of the air stream is determined from the measured temperature and relative humidity of the air stream and the vapor density at the surface of the water is determined from the measured temperature of the water and the assumption of saturation at the surface.

The schematic of the test section is shown in Fig. 1. This is a 3D rectangular duct with a dimension of $W \times H \times L$ as 298 mm × 20.5 mm × 600 mm. At the bottom of the test section which is 298 mm in width, a tray with a water surface of 280 mm width (b) is placed in the middle. The remaining 18 mm in bottom boundary is insulated with 9 mm in each side. The other three walls of the ducts are insulated. The air is delivered to the test section from an environmental chamber that controls the temperature and relative humidity of the air upstream of the test section within ±0.1 °C and ±2% RH, respectively.

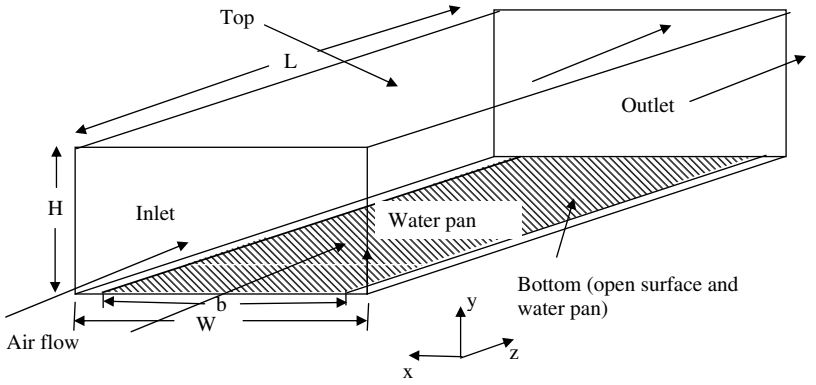

Fig. 1. Schematic of the problem under consideration.

3. Numerical modeling

The governing transport equations in 3D Cartesian coordinates for the fluid flow, heat and mass transfer are given below with the following assumptions:

- Flow is considered to be steady and laminar.
- Viscous dissipation and compressibility effects in the energy equation are neglected.
- The thermophysical properties of the fluid are assumed to be constant except the density which is allowed to vary in the buoyancy term of the y-momentum equation.
- The secondary effects of concentration gradient on thermal diffusion and of thermal diffusion on mass transfer have been neglected.

Continuity:

$$\frac{\partial u}{\partial x}+\frac{\partial v}{\partial y}+\frac{\partial w}{\partial z}=0 \tag{1}$$

x-Momentum:

$$\left[u\frac{\partial u}{\partial x}+v\frac{\partial u}{\partial y}+w\frac{\partial u}{\partial z}\right]=-\frac{1}{\rho}\frac{\partial p}{\partial x}+\nu\left[\frac{\partial^2 u}{\partial x^2}+\frac{\partial^2 u}{\partial y^2}+\frac{\partial^2 u}{\partial z^2}\right] \tag{2}$$

y-Momentum:

$$\left[u\frac{\partial v}{\partial x}+v\frac{\partial v}{\partial y}+w\frac{\partial v}{\partial z}\right]=-\frac{1}{\rho}\frac{\partial p}{\partial y}+\nu\left[\frac{\partial^2 v}{\partial x^2}+\frac{\partial^2 v}{\partial y^2}+\frac{\partial^2 v}{\partial z^2}\right]+\beta g(T-T_0)+\beta^* g(C-C_0) \tag{3}$$

z-Momentum:

$$\left[u\frac{\partial w}{\partial x}+v\frac{\partial w}{\partial y}+w\frac{\partial w}{\partial z}\right]=-\frac{1}{\rho}\frac{\partial p}{\partial z}+\nu\left[\frac{\partial^2 w}{\partial x^2}+\frac{\partial^2 w}{\partial y^2}+\frac{\partial^2 w}{\partial z^2}\right] \tag{4}$$

Energy:

$$\left[u\frac{\partial T}{\partial x}+v\frac{\partial T}{\partial y}+w\frac{\partial T}{\partial z}\right]=\alpha\left[\frac{\partial^2 T}{\partial x^2}+\frac{\partial^2 T}{\partial y^2}+\frac{\partial^2 T}{\partial z^2}\right] \tag{5}$$

Concentration:

$$u\frac{\partial C}{\partial x}+v\frac{\partial C}{\partial y}+w\frac{\partial C}{\partial z}=D_{\mathrm{AB}}\left[\frac{\partial^2 C}{\partial x^2}+\frac{\partial^2 C}{\partial y^2}+\frac{\partial^2 C}{\partial z^2}\right] \tag{6}$$

In the above equations, u, v and w are the velocity components in x, y and z directions, p, T and C is the pressure, temperature and vapor density/concentration of the flowing air. Buoyancy forces created by both temperature and concentration gradient are considered and are included in the y-momentum equation. The volumetric coefficient of thermal expansion β is given by

$$\beta=-\frac{1}{\rho}\frac{\partial \rho}{\partial T}=\frac{1}{T} \tag{7}$$

and the species expansion coefficient β^* is given by,

$$\beta^*=-\frac{1}{\rho}\frac{\partial \rho}{\partial C}=\frac{1}{\rho}\left[\frac{\mathrm{MW_a}}{\mathrm{MW_v}}-1\right] \tag{8}$$

where $\mathrm{MW_a}$ and $\mathrm{MW_v}$ are the molecular weights of air and water vapor, respectively. In the simulations, β and β^* for air are taken approximately as 0.00343 ($1/K$) and 0.513 ($\mathrm{m^3/kg}$) based on reference temperature and vapor density. The reference temperature T_0 and concentration C_0 are taken as the inlet temperature and vapor density of air, respectively.

The boundary conditions for the problem are:

Inlet (*at* $z=0$):

Momentum: a fully developed velocity profile of air is assumed at the entrance which can be mathematically expressed as [32]:

$$\frac{w}{w_{\mathrm{av}}}=\left(\frac{m+1}{m}\right)\left(\frac{n+1}{n}\right)\left[1-\left(\frac{y}{H}\right)^n\right]\left[1-\left(\frac{x}{W}\right)^m\right] \tag{9}$$

and $u=v=0$ (10)

where,

$$m=1.7+0.5(\gamma)^{-1.4}$$

$$n=2 \quad \text{for } \gamma\leqslant 1/3$$

$$=2+0.3(\gamma-1/3) \quad \gamma\geqslant 1/3$$

$\gamma(=W/H=14.54)$ is the aspect ratio of the duct. The average velocity $w_{av}$is based on the specified Reynolds numbers.

$$w_{av}=\frac{Re\mu}{\rho D_h} \tag{11}$$

where the hydraulic diameter D_h is based on the wetted perimeter.

$$D_h=\frac{4WH}{2(W+H)} \tag{12}$$

$$Energy: T=T_0 \text{ (specified)} \tag{13}$$

$$Concentration: C=C_0 \text{ (specified)} \tag{14}$$

C_0 is the vapor density/concentration of air corresponding to the given inlet temperature T_0 and specified relative humidity

Top and side walls (*at* $x=0$, $x=W$ and $y=H$):

$$Momentum: \text{no slip}(u=v=w=0) \tag{15}$$

$$Energy: \text{adiabatic}\left(\frac{\partial T}{\partial n}=0.0\right) \tag{16}$$

$$Concentration: \text{impermeable}\left(\frac{\partial C}{\partial n}=0.0\right) \tag{17}$$

where n is the direction perpendicular to the boundary.

Bottom wall (at $y=0$):

$$Momentum: \text{no slip}(u=v=w=0) \tag{18}$$

The interfacial velocity at the bottom wall as a result of mass diffusion process is neglected here. The validity and the condition for the neglect of interfacial velocity has been discussed in [18,19].

Energy: It is assumed that the amount of heat of phase change required for the evaporation of water is equal to the sensible heat transfer from the air to the water surface. This gives a boundary condition at the bottom surface as:

$$-k\left.\frac{\partial T}{\partial y}\right|_{y=0}=h_{fg}D_{AB}\left.\frac{\partial C}{\partial y}\right|_{y=0} \tag{19}$$

where k is the thermal conductivity of air, D_{AB} is the binary diffusion coefficient of water vapor in air and $h_{fg}$is the heat of phase change of water.

Concentration: Based on the temperature at $y=0$ (water temperature T_w) which is calculated using Eq. (19) and assuming fully saturated condition (100% relative humidity) at this water temperature, the vapor density is calculated.

$$C=C_{sat}=f(T_w) \tag{20}$$

As mentioned in the previous section that the size of the water tray b (280 mm) is slightly narrower than the width W (298 mm) of the duct. In simulations, Eqs. (19) and (20) are applied for the 280 mm width and in the rest of the bottom boundary (9 mm each side in the x direction), adiabatic and impermeable boundary condition given by Eqs. (16) and (17) is applied.

Outlet ($z=L$): Vanishing gradients are assumed at the outlet for momentum, energy and concentration.

$$\frac{\partial u}{\partial z}=\frac{\partial v}{\partial z}=\frac{\partial w}{\partial z}=\frac{\partial T}{\partial z}=\frac{\partial C}{\partial z}=0 \tag{21}$$

Local and average Nu and Sh will be presented. The local or cross sectional averaged Nu and Sh at every z location (in the main flow direction) are calculated averaging over the entire cross section perpendicular to the main flow (z) direction as:

$$Nu_z=\frac{-\left.\frac{\partial T}{\partial y}\right|_{y=0}}{T_w-T_m}D_h \tag{22}$$

$$Sh_z=\frac{-\left.\frac{\partial C}{\partial y}\right|_{y=0}}{C_w-C_m}D_h \tag{23}$$

T_w and C_w are the temperature and vapor density of air at the bottom boundary and T_m and C_m are the bulk mean temperature and bulk mean vapor density respectively. The average Nusselt and Sherwood number is calculated as:

$$Nu_{av}=\int_0^z\frac{-\left.\frac{\partial T}{\partial y}\right|_{y=0}}{\Delta T}dz \tag{24}$$

$$Sh_{av}=\int_0^z\frac{-\left.\frac{\partial C}{\partial y}\right|_{y=0}}{\Delta C}dz \tag{25}$$

where ΔT and ΔC is the log mean temperature and vapor density difference of air. ΔT can be defined as

$$\Delta T=\frac{(T_w-T_z)-(T_w-T_0)}{\ln[(T_w-T_z)/(T_w-T_0)]} \tag{26}$$

ΔC can be defined in a similar way.

3.1. Solution procedure

The governing equations are solved using an 'in-house' code FASTEST3D (flow analysis by solving transport equations simulating turbulence) developed at the Institute of Fluid Mechanics, University of Erlangen-Nuremberg, Germany. The code is based on the finite volume method and is written in curvilinear coordinates. It employs the methodology of block structured grid to handle complex geometries. SIMPLE algorithm is used for solution of momentum equations. The code can be run on multiple processors and capable of multigrid approach. The variable arrangement is collocated. Diffusive fluxes are discretized using a central differencing scheme. Deferred correction approach between central differencing and upwind differencing scheme is used for the convective fluxes. The resulting system of algebraic equations is solved through the semi-infinite procedure according to Stone. The basic procedure for the three-dimensional formulation is described in [33]. The solution domain is discretized by a structured mesh of hexahedral elements. The number of control volumes used for the calculations are $50\times50\times100$ based on a study that they give reasonable agreement with the already published data. A non-uniform grid is used with a

finer control volume closer to the wall and in the entrance of the duct.

4. Results and discussion

4.1. Validation with numerical data in the literature

The code is first validated with three different cases reported in the literature. First, a case of forced convection heat transfer in a square duct is considered. The flow is hydrodynamically fully developed and thermally developing. All four walls are kept at constant temperature. Results of the local Nusselt number (Nu_z) along the non-dimensional axial length $z/(RePrD_h)$ are compared with the results of Lyczkowski et al. [31]. As seen from Fig. 2, a good agreement is observed.

In the second case, a combined forced and natural convection problem is chosen. A square duct with a constant and uniform temperature and concentration at the boundaries is selected. The fluid enters the duct with a fully developed velocity profile and constant temperature and concentration. The Rayleigh number

$$Ra = \frac{g\beta(T_w - T_0)\rho^2 C_p D_h^3}{\mu k} \tag{27}$$

which signifies the relative importance of buoyancy force is 5×10^4 and Prandtl ($Pr = \nu/\alpha$) and Schmidt number ($Sc = \nu/D_{AB}$) are 0.71 and 0.6, respectively. Since this is a case of simultaneous of heat and mass transfer, the buoyancy ratio

$$N = \frac{\beta^*(C_w - C_0)}{\beta(T_w - T_0)} \tag{28}$$

considered is 1. The results presented in Fig. 2 shows a good agreement between the present work and the work of Yan [20].

The third comparison is done for a rectangular duct of aspect ratio 10. Three walls of the duct are adiabatic and one (one of the longer walls) is at a constant temperature. The flow is hydrodynamically fully developed and thermally developing. The asymptotic Nusselt number is found to be 4.32 which compares favorably to the value of 4.27 determined by Schmidt [32].

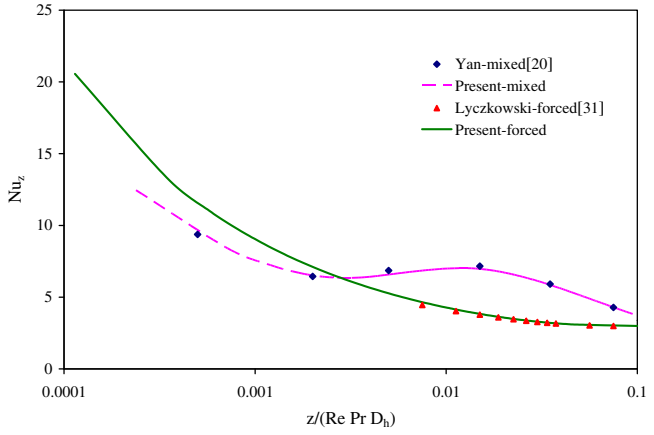

Fig. 2. Validation of the present work with the literature.

4.2. Validation with experimental data

In Table 1, inlet temperature, relative humidity and *Re* are specified for the experiments done [23] in laminar regime. Numerical simulations are performed for these specific cases. Fig. 3a compares the experimental and numerical data for water temperature (T_w) and the temperature and RH at the outlet of the test section for the 10 laminar flow tests given in Table 1. It is seen from the figure that water temperature lies in the range of 10–16 °C (12–17.5 °C in the experiments) for the inlet temperature imposed in the range of 22–23 °C. The temperature of the water reduces because of the loss of heat due to the evaporation of water. The outlet temperature slightly reduces because of the cold water at the bottom. This can be seen more clearly later from the isotherms of Fig. 5. The water temperature depends on the inlet temperature and RH of air stream. Since the inlet temperature is relatively same for all the cases, it is the inlet RH which mainly decides the water temperature. For higher inlet RH, there will be less evaporation from water to the air stream resulting a higher water temperature as seen from the cases 9 and 10 of Fig. 3a. The relative humidity of air at the outlet increases because of evaporation of water from the pan. It can be seen from Fig. 3a that T_w found from the simulation is an average 1.8 °C lower than that measured in the experiment. This indicates that there could be a heat gain from surroundings which will be discussed later in the sensitivity section. Another reason for the difference between the experimental and numerical data could be errors in the measurement of the water temperature in the experiments. This will also be discussed in the sensitivity section. Fig. 3a shows that the experimental and numerical data for temperature at the downstream of the test section (outlet) are close to each other with an average difference of 0.5 °C and maximum difference of 1.3 °C. The other comparison is the RH at the downstream of the test section (outlet). In all cases (except case 1), the experimental values are lower than the numerical values. The average and max-

Table 1
Inlet conditions for different experiments performed

Cases	*Re*	Inlet air RH (%)	Inlet air temperature T_0 (°C)
1	2079	17.9	22.9
2	1863	25.4	23.1
3	1583	19.7	22.7
4	1340	23.0	22.8
5	796	17.2	22.3
6	1303	35.2	22.1
7	2059	34.5	22.3
8	699	33.6	21.9
9	844	53.1	22.4
10	1531	54.7	22.0

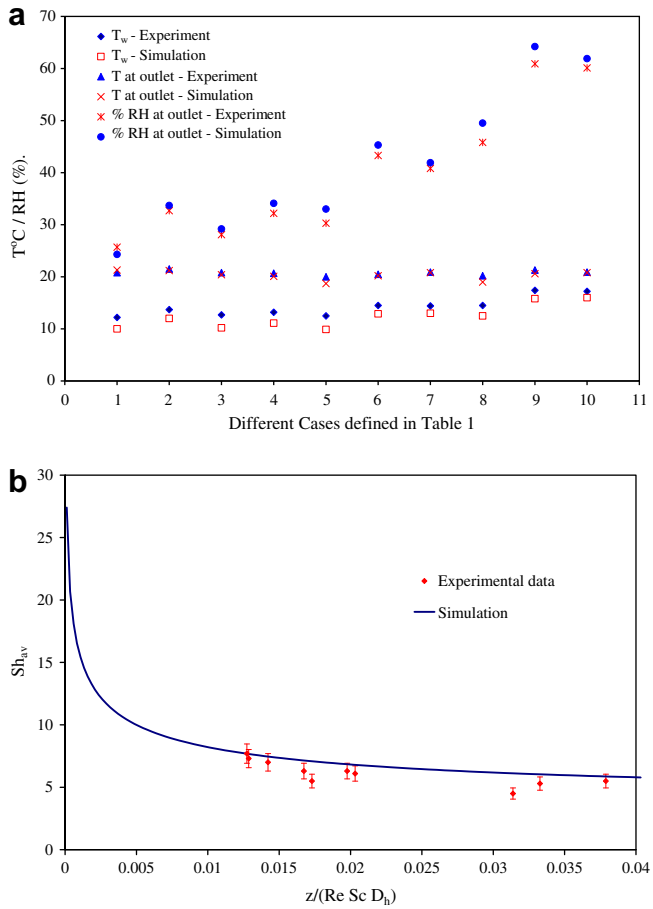

Fig. 3. Comparison of numerical and experimental data for (a) water temperature T_w, outlet temperature and RH (b) Sherwood number.

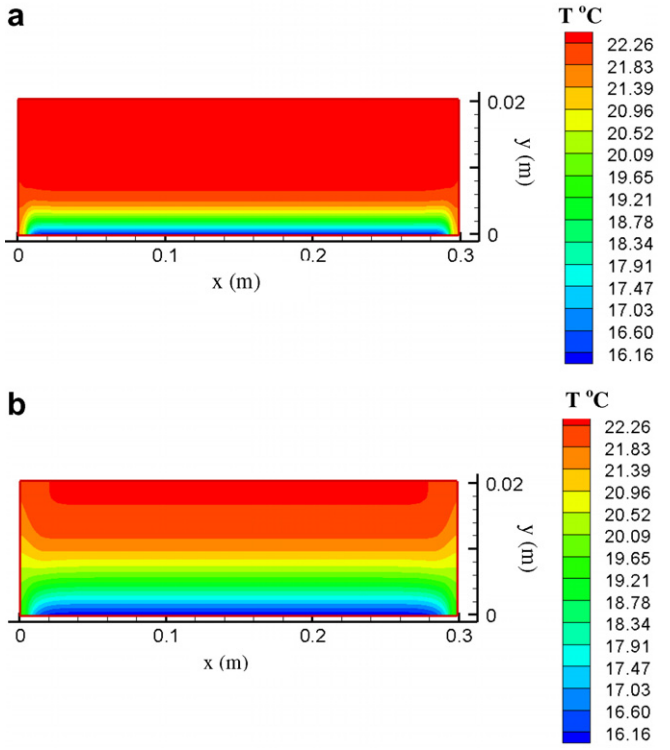

Fig. 4. Isotherms at different z location, (a) $z = 0.05$ m and (b) $z = 0.45$ m for case 9 of Table 1.

imum differences between the experimental and numerical data are 1.9% and 3.7%. The maximum differences occur in the low *Re* cases.

Fig. 3b compares experimental and numerical data of Sh_{av} and includes a ±10% error bars for the experimental data which is average 95% uncertainty bounds for most of the experimental data. It is seen that numerical data are within the experimental uncertainty range for most of the tests. The numerical results that are outside the experimental error bounds are cases 9 and 10 (Table 1) which have a higher inlet RH. The trend of Sh_{av} distribution indicates dominance of forced convection over natural convection. As the concentration boundary layer approaches to a fully developed state, Sh_Z (and Sh_{av}) approaches to an asymptotic value. Presence of natural convection enhances the heat and mass transfer processes which results in an increase of Nu_z, Sh_z (Nu_{av}, Sh_{av}) distribution in the downstream, followed by a decrease in the further downstream before it approaches to a fully developed state (see Fig. 2 for such a behavior for the mixed convection case). In the present study such a behavior could not be seen which indicates absence of natural convection.

To investigate the absence of natural convection further, isotherms are plotted in Fig. 4 at two different z locations. This particular case is for $Re = 844$ (Table 1), but it is found that the trends are similar for all cases. As seen from the figure that the side wall temperature is influenced by the cold water which creates a week secondary flow. However this is not enough and forced convection is the dominant mode of heat transfer for this problem. Natural convection due to concentration gradient is also quite weak to have any effect on Sh_{av}.

4.3. Boundary layer development and heat and mass transfer analogy

In Fig. 5, contours for temperature and vapor concentration at $x = W/2$ plane are shown for case 9 of Table 1. It is seen from both figures that the thermal and concentration boundary layer are developing. As found from correlation in many of the heat transfer text books that the fully developed length of laminar thermal boundary layer for a duct of $D_h = 0.0384$ m, $Re = 844$ and $Pr = 0.71$ is more than 1 m. The concentration boundary layer is slightly shorter as *Sc* is 0.59 but still longer than the 0.6 m length shown in Fig. 5b. *Pr* being higher than *Sc*, thermal boundary layer develops slower than the concentration boundary layer and as a result *Nu* is higher than *Sh* for this case which can be seen in Fig. 6 where local Nu_z and Sh_z are presented. In many of the heat transfer text books the analogy between heat and mass transfer is discussed and it has been shown that *Nu* and *Sh* is related to each other by

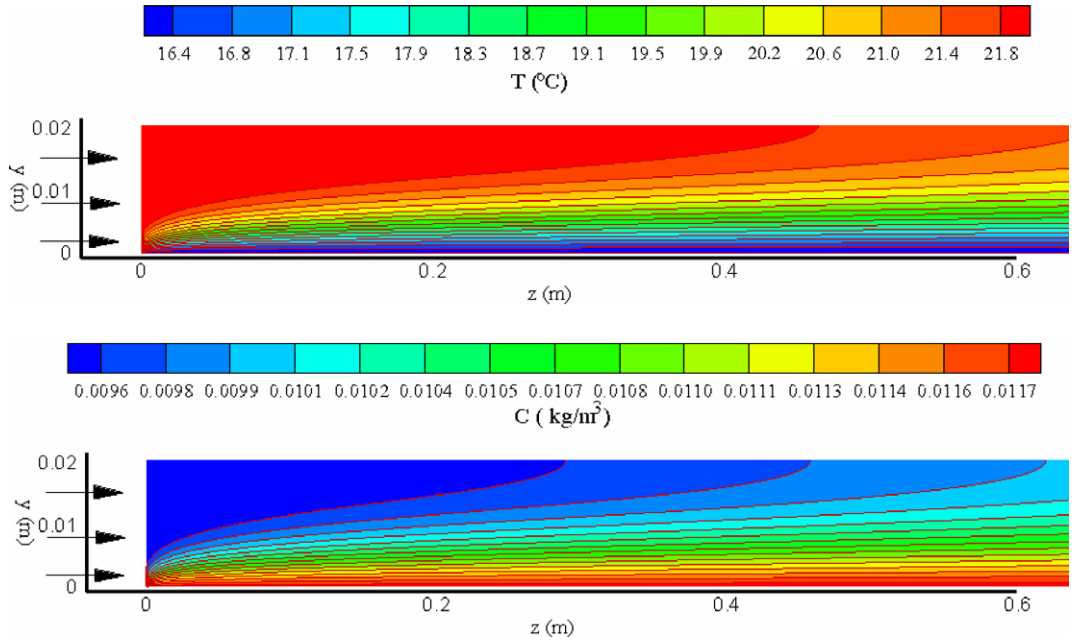

Fig. 5. Contours of temperature and vapor density of air for $Re = 844$ (case 9, Table 1).

$$\frac{Nu}{Sh} = \left(\frac{Pr}{Sc}\right)^n \tag{30}$$

where $n \cong 1/3$ for most of the cases. In the present case a similar analogy is defined based on the fact that the latent heat of evaporation of water is equal to the sensible heat transfer from the air to the water (Eq. (19)) as all the boundaries of the duct are insulated. This gives a relation followed by (Eq. (19)),

$$\begin{aligned} -k\frac{\partial T}{\partial y}\bigg|_{y=0} &= h_{fg} D_{AB} \frac{\partial C}{\partial y}\bigg|_{y=0} \Rightarrow \frac{-\frac{\partial T}{\partial y}\big|_{y=0} D_h}{\Delta T} \\ &= \frac{-\frac{\partial C}{\partial y}\big|_{y=0} D_h}{\Delta C} \cdot \left(-\frac{D_{AB} h_{fg} \Delta C}{k \Delta T}\right) \Rightarrow Nu_{av} \\ &= Sh_{av} \cdot (-S^*) \end{aligned} \tag{31}$$

Here S^* is a dimensionless parameter which shows the ratio between heat and mass transfer and its value can be different for different fluids depending on their properties. For the present cases, the value of S^* is found in the ranges of -1.06 to -1.08. In simulations, it has been verified that the ratio of Nu_{av} and Sh_{av} is equal to $S^* (= D_{AB} h_{fg} \Delta C/(k\Delta T))$. In the experiments [23], since only Sh_{av} are calculated, Nu_{av} can be calculated using the above relation. However, the value of S^* is found to be quite low (in the range of -1.7 to -2.3 shown in Table 2) in the experiments which gives a very high Nu_{av}. The two possibilities (similar to the explanation for disagreement in Fig. 3a) could be heat gain by the water from surroundings or a measurement error of water temperature which are discussed in the next section.

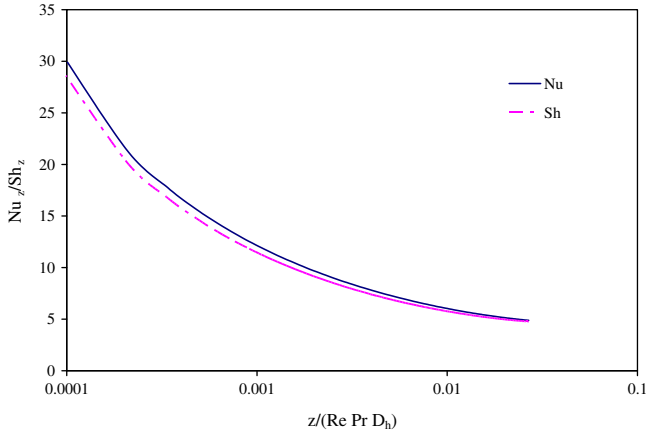

Fig. 6. Local Nusselt and Sherwood number distribution.

4.4. Sensitivity studies

To examine the effect of heat gain or loss from the surroundings on the numerical data, different external heat fluxes q (W/m^2) are applied at the water surface ($y = 0$).

Table 2
Data and sensitivity study on S^*

Re	S^* (experimental)	S^* (experimental) reducing T_w by 1 °C	S^* (experimental) reducing T_w by 1.5 °C	S^* (simulation)
699	−1.7	−1.4	−1.2	−1.06
1303	−1.9	−1.4	−1.2	−1.07
1340	−1.8	−1.4	−1.3	−1.07
1583	−1.8	−1.4	−1.3	−1.06
1863	−1.7	−1.3	−1.2	−1.08
2059	−1.8	−1.3	−1.1	−1.08
2079	−1.7	−1.3	−1.2	−1.06
796	−1.9	−1.5	−1.4	−1.06
844	−2.1	−1.3	−1.1	−1.06
1531	−2.3	−1.4	−1.1	−1.08

Results are generated for $q = \pm 10$, ± 50, ± 100 W/m^2 and are presented in Figs. 7–9. In Fig. 7a, Nu_{av}, Sh_{av} and S^* are presented for the entire duct length of 0.6 m. It is seen from the figure that $-S^*$ increases to a maximum of 1.9 or in the other way S^* decreases to a minimum of -1.9 for $q = 100$ W/m^2. For $q = -100$, ± 50 and 10, Sh_{av} is found to be greater than Nu_{av} and hence results in a value of S^* less than -1. This study shows that if there is a heat gain or loss through the bottom surface, S^* could have a considerably different value than (-1.06) to (-1.08) range for the adiabatic cases discussed before. This indicates one possible reason of getting different S^* and Sh_{av} in the experiments.

Nu_{av} and Sh_{av} along the axial length z of the duct are presented in Fig. 7b and c, respectively for $q = \pm 100$, ± 50 W/m^2. It can be seen from Fig. 7b that for $q = 100$ W/m^2, Nu_{av} becomes negative and then increases sharply to a maximum value and then gradually decreases. Similar trend for Sh_{av} is seen in Fig. 7c for $q = -100$ and -50 W/m^2. The reason for such a behavior can be explained with Fig. 8a and b where temperature and vapor density distribution along the main flow direction (z) is shown. In both the figures, cases with $q = 100$, -50 W/m^2 is chosen. In Fig. 8a, bulk mean temperature of air T_m and water temperature T_w is plotted whereas in Fig. 8b, bulk mean vapor density C_m and vapor density at the water surface C_w is plotted. It is seen from Fig. 8a that for $q = 100$ W/m^2, water temperature increases from 17 to 25 °C because of this constant and uniform heat flux at the water surface. The change in T_m is quite low along the z direction and T_w and T_m profile crosses each other in a location near the inlet. While calculating the Nu, the average temperature gradient at the bottom wall is considered. The sign of $-k\partial T/\partial y$ and ΔT is normally same which produces a positive Nu number always. But in the present case, because of the imposed heat flux at the bottom, $-k\partial T/\partial y$ and ΔT bear opposite sign for a certain length closer to the intersection of T_w and T_m plots. This is happened because at the locations along z direction when T_m approaches the value of T_w and becomes eventually lower than T_w, the temperature at the locations closer to the wall (than T_m) approaches a little bit ahead the value of T_w. So, for a certain length along z direction, though T_m is higher than T_w, the temperature closer to the wall already attains a value lower than T_w. This results an opposite sign for $-k\partial T/\partial y$ and ΔT for this region producing a negative Nu. To explain this phenomena further, center line (at $x = 0.149$ m) temperature profile along y direction is presented in Fig. 9 at different axial locations $z = 0.1$, 0.18 and 0.3 m. It is seen from the figure that at locations $z = 0.18$ m, there is a reversal of temperature plots. It decreases and then increases again along y direction. Because of this, even T_m is higher than T_w (not shown) at this location, temperature at the location closer to the wall can be lower than T_w which results a positive $-k\partial T/\partial y$ (ΔT is negative) and a negative Nu therefore. The temperature profile at the two other locations does not have

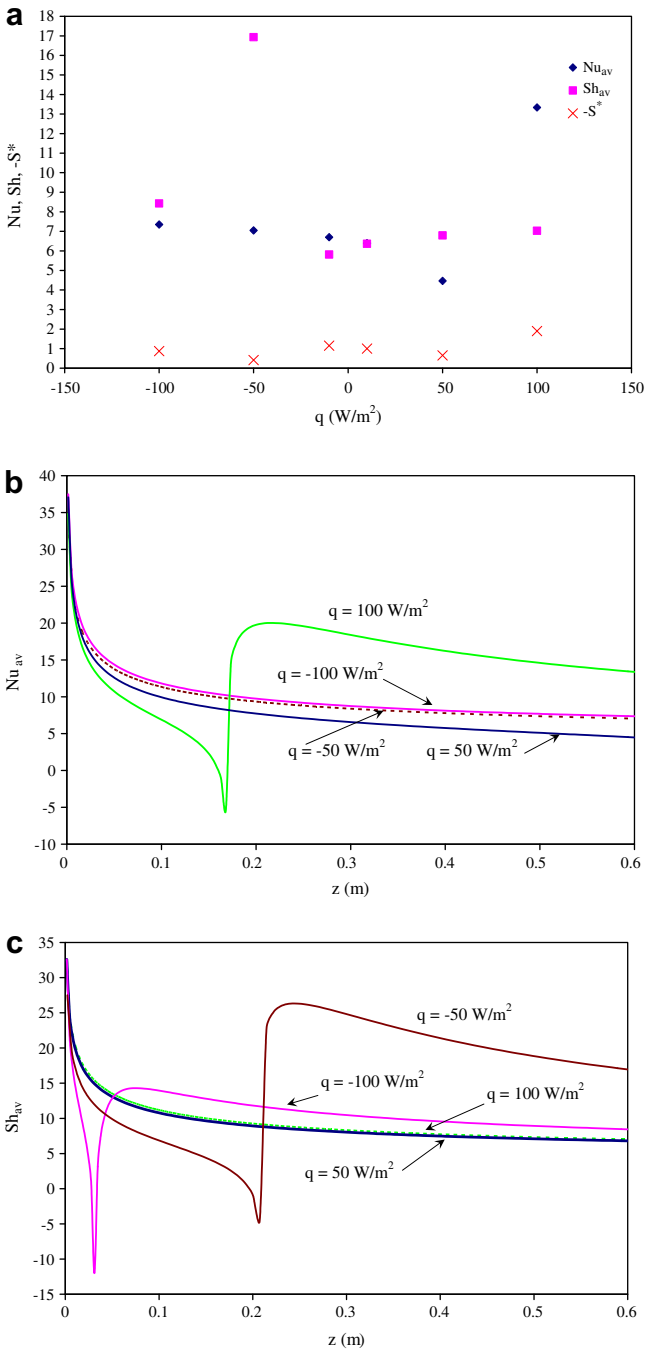

Fig. 7. Effect of imposing heat flux at the water surface ($y = 0$) on S^*, Nu_{av} and Sh_{av}.

a sharp reversal trend and as such a positive Nu is observed in Fig. 7b.

It can be seen from Fig. 8a that for $q = -50$ W/m^2 (also for the other cases taken in Fig. 7b which are not shown in Fig. 8), T_m and T_w both decreases (there is no intersection of these two profiles) and hence no such jumps in Nu_{av} is observed in Fig. 7b. We will also not see any temperature reversal for these cases.

In Fig. 8b, for $q = -50$ W/m^2, similar intersection takes place between C_m and C_w resulting in a jump in Sh_{av} num-

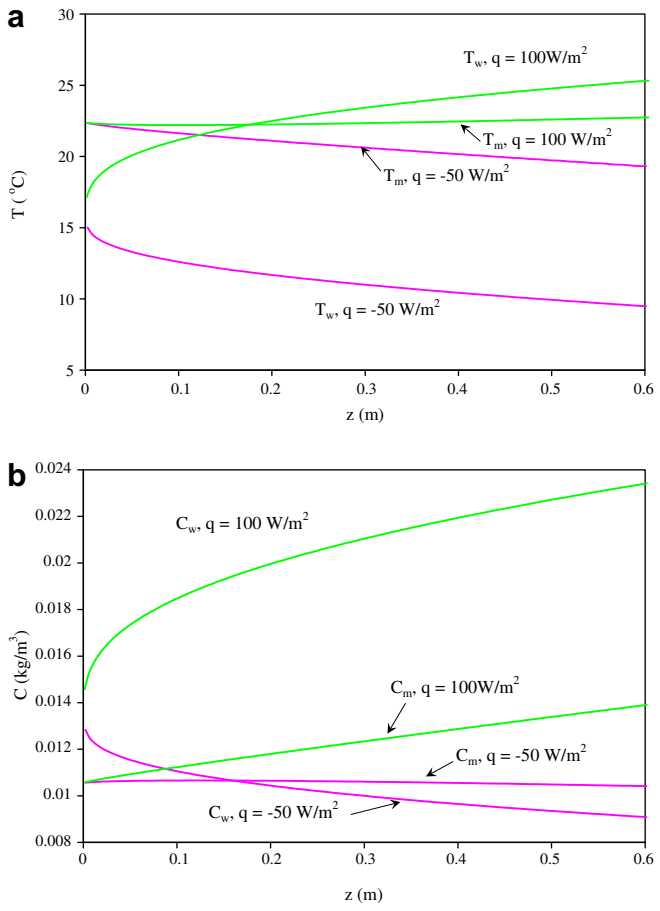

Fig. 8. Effect of imposing heat flux at the water surface ($y = 0$) on T (a) and C (b).

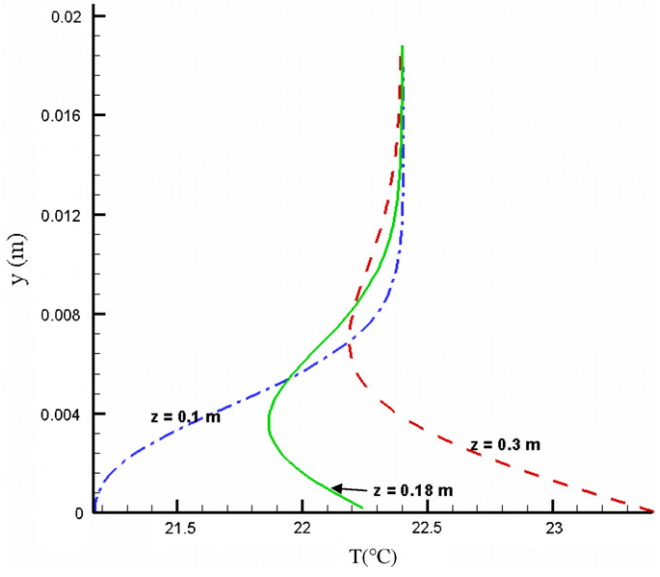

Fig. 9. Temperature profiles along the y direction at the centerline (at $x = 0.149$ m) and at different axial locations $z = 0.1$, 0.18, 0.3 m with an imposed heat flux of $q = 100$ W/m^2.

ber (Fig. 7c). This behavior can be explained in a similar way as done for Nu. The reason for a decreasing trend of C_w along z direction is that T_w decreases along z (Fig. 8a) for $q = -50$ W/m^2 (recall Eq. (20)). The changes in C_m is quite low although a close observation shows that it increases first (because C_w is higher than C_m near to the inlet) and then starts decreasing towards the outlet with C_w. In the current simulation, a constant heat flux is applied at the bottom surface and conduction at the water surface is not considered. In practical cases, conduction at the water surface may play a role making temperature at the water surface almost uniform. This might eliminate the occurring of a jump of Nu or Sh and could give a higher uniform temperature at the water surface than numerically found for the adiabatic cases and could bring the matching between numerical and experimental data closer.

As indicated before, the error in the measurement of water temperature in experiments could considerably change the results of Sh_{av} and S^* and could improve the agreement between experimental and numerical data. A study is carried out by reducing the water temperature of experimental data by 1.0 and 1.5 °C and then recalculating Sh and S^* keeping the other conditions same. The corresponding effect on Sh_{av} and S^* is shown in Fig. 10 and Table 2, respectively. It is seen from Fig. 10 that reducing T_w by 1 °C brings the experimental data closer to the simulation data especially for the cases of high inlet RH (the last two cases in Table 1) which were not in good agreement before. For S^*, it is observed from Table 2 that reduction of T_w by 1.5 °C brings the experimental S^* data closer to the numerically found S^*. In addition to Fig. 10, Table 3 shows the exact amount of T_w to be reduced in experimental data to get Sh_{av} (experimental) = Sh_{av} (numerical). It is seen that the value lies in the range of 0.1–1.3.

Sensitivity of inlet velocity profile on Sh_{av} is studied in Fig. 11 to investigate another probable reason of disagreement between experimental and numerical Sh. In the simulations, it is assumed that the velocity profile at the inlet is fully developed. But there is always a chance that the flow may not be completely fully developed. A sensitivity study is carried out with the shape of the inlet velocity profile in Fig. 11. It is seen that the uniform velocity at the inlet pro-

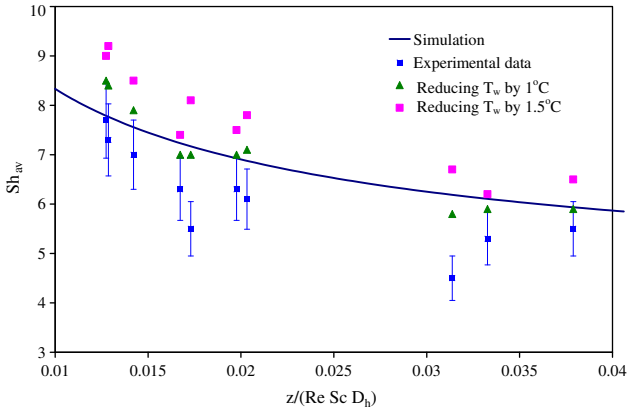

Fig. 10. Effect of water temperature T_w on Sh_{av}.

Table 3
Amount of T_w to be reduced in experimental data to get Sh_{av} (experimental) = Sh_{av} (numerical)

Re	699	1303	1340	1583	1863	2059	2079	796	844	1531
T_w to be reduced	0.5	0.8	0.8	1.4	0.6	0.4	0.1	1.3	1.2	1.0

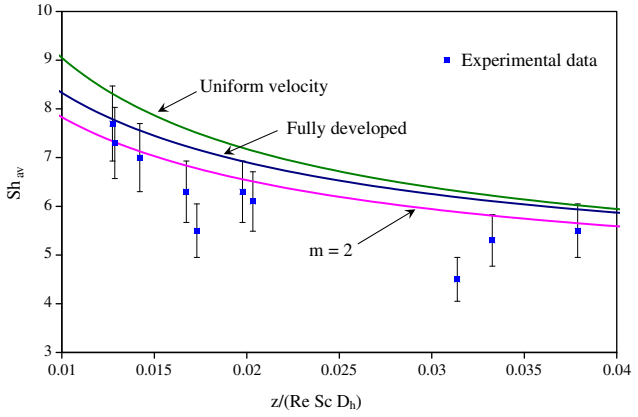

Fig. 11. Effect of velocity profile on Sh_{av} number.

duces maximum Sh_{av} as expected. But a velocity profile with index $m = 2$ in Eq. (9), produces a lower Sh_{av} than a fully developed velocity profile ($m = 22.6$) especially at the entrance section. So, if the inlet velocity profile is not fully developed rather close to the case of $m = 2$, Sh_{av} with numerical simulation could come closer to the experimental data.

5. Conclusions

This paper presents numerical simulation of heat and mass transfer in a short rectangular duct. Three-dimensional CFD simulations were carried out with laminar flow. The experimental and numerical data were compared and possibilities of their disagreement were discussed with different sensitivity studies. The findings can be summarized as:

- Numerical data fall within the uncertainty range for most of the experimental data.
- Introducing heat gain/loss at the water surface could produce negative Nusselt or Sherwood number for this combined heat and mass transfer process.
- The effects of buoyancy forces were found to be negligible.
- Heat and mass transfer analogy is defined with a new relation.

Acknowledgements

Funding from Natural Science and Engineering Research Council of Canada (NSERC) Discovery and Special Research Opportunity Programs as well as Canada Foundation for Innovation (CFI) are greatly appreciated.

References

[1] C.J. Simonson, M. Salonvaara, T. Ojanen, Heat and mass transfer between indoor air and a permeable and hygroscopic building envelope. Part I. Field measurements, J. Therm. Envelope Build. Sci. 28 (1) (2004) 63–101.
[2] P. Talukdar, S.O. Olutmayin, O.F. Osanyintola, C.J. Simonson, An experimental data set for benchmarking 1D, transient heat and moisture transfer models of porous building materials. Part I. Experimental facility and material property data, Int. J. Heat Mass Transfer 50 (2007) 4527–4539.
[3] P. Talukdar, O.F. Osanyintola, S.O. Olutmayin, C.J. Simonson, An experimental data set for benchmarking 1-D, transient heat and moisture transfer models of porous building materials. Part II. Experimental, numerical and analytical data, Int. J. Heat Mass Transfer (2007).
[4] A.K. Datta, Porous media approaches to studying simultaneous heat and mass transfer in food processes. II. Property data and representative results, J. Food Eng. 80 (1) (2007) 96–110.
[5] Y. Xia, A.M. Jacobi, Air-side data interpretation and performance analysis for heat exchangers with simultaneous heat and mass transfer: wet and frosted surfaces, Int. J. Heat Mass Transfer 48 (2005) 5089–5102.
[6] H. Sadek, A.J. Robinson, J.S. Cotton, C.Y. Ching, M. Shoukri, Electrohydrodynamic enhancement of in-tube convective condensation heat transfer, Int. J. Heat Mass Transfer 49 (2006) 1647–1657.
[7] R. Yun, Y. Kim, M.S. Kim, Convective boiling heat transfer characteristics of CO_2 in microchannels, Int. J. Heat Mass Transfer 48 (2005) 235–242.
[8] S.O. Olutimayin, C.J. Simonson, Measuring and modeling vapor boundary layer growth during transient diffusion heat and moisture transfer in cellulose insulation, Int. J. Heat Mass Transfer 48 (2005) 3319–3330.
[9] K.C. Cheng, G.J. Hwang, Numerical solution for combined free and forced laminar convection in horizontal rectangular channels, J. Heat Transfer 91 (1969) 59–66.
[10] K.C. Cheng, S.W. Hong, G.J. Hwang, Buoyancy effects on laminar heat transfer in the thermal entrance region of horizontal rectangular channels with uniform wall heat flux for large Prandtl number fluid, Int. J. Heat Mass Transfer 15 (1972) 1819–1836.
[11] J.W. Ou, K.C. Cheng, R.C. Lin, Natural convection effects on Graetz problem in horizontal rectangular channels with uniform wall temperature for large *Pr*, Int. J. Heat Mass Transfer 17 (1974) 835–843.
[12] C.A. Hieber, S.K. Sreenivasan, Mixed convection in an isothermally heated horizontal pipe, Int. J. Heat Mass Transfer 17 (1974) 1337–1348.
[13] M. Hishida, Y. Nagano, M.S. Montesclaros, Combined forced and free convection in the entrance region of an isothermally heated horizontal pipe, J. Heat Transfer 105 (1982) 153–159.
[14] G.J. Hwang, C.L. Liu, An experimental study of convective instability in the thermal entrance region of a horizontal parallel plate channel heated from below, Can. J. Chem. Engng. 54 (1976) 521–525.
[15] J.R. Maughan, F.P. Incropera, Experiments on mixed convection heat transfer for airflow in a horizontal and inclined channel, Int. J. Heat Mass Transfer 30 (1987) 1307–1318.
[16] T.F. Lin, C.J. Cheng, W.M. Yan, Analysis of combined buoyancy effects of thermal and mass diffusion on laminar forced convection heat transfer in a vertical tube, J. Heat Transfer 110 (1988) 337–344.
[17] J.N. Lin, F.C. Chou, W.M. Yan, P.Y. Tzeng, Combined buoyancy effects of thermal and mass diffusion on laminar forced convection in

the thermal entrance region of horizontal square channels, Can. J. Chem. Engng 79 (1992) 681–689.
[18] B. Gebhart, L. Pera, The nature of vertical natural convection flows resulting from the combined buoyancy effects of thermal and mass diffusion, Int. J. Heat Mass Transfer 14 (1971) 2025–2050.
[19] T.S. Chen, C.F. Yuh, Combined heat and mass transfer in natural convection along a vertical cylinder, Int. J. Heat Mass Transfer 23 (1980) 451–461.
[20] W.M. Yan, Combined buoyancy effects of thermal and mass diffusion on laminar forced convection in horizontal rectangular ducts, Int. J. Heat Mass Transfer 39 (1996) 1479–1488.
[21] J.N. Lin, P.Y. Tzeng, Convective instability of heat and mass transfer for laminar forced convection in the thermal entrance region of horizontal rectangular channels, Int. J. Heat Fluid Flow 13 (3) (1992) 250–258.
[22] A. Kaya, O. Aydin, I. Dincer, Numerical modeling of heat and mass transfer during forced convection drying of rectangular moist objects, Int. J. Heat Mass Transfer 49 (2006) 3094–3103.
[23] C.R. Iskra, C.J. Simonson, Convective mass transfer coefficient for a hydrodynamically developed airflow in a short rectangular duct, Int. J. Heat Mass Transfer 50 (2007) 2376–2393.
[24] M.M.M. Abou-Ellail, S.M. Morcos, Buoyancy effects in the entrance region of horizontal rectangular channels, J. Heat Transfer 105 (1983) 924–928.
[25] F.P. Incropera, J.A. Schutt, Numerical simulation of laminar mixed convection in the entrance region of horizontal rectangular ducts, Numer. Heat Transfer 8 (1985) 707–729.
[26] H.V. Mahney, F.P. Incropera, S. Ramadhyani, Development of laminar mixed convection flow in a horizontal rectangular duct with uniform bottom heating, Numer. Heat Transfer 12 (1987) 137–155.
[27] J.N. Lin, F.C. Chou, Laminar mixed convection in the thermal entrance region of horizontal isothermal rectangular channels, Can. J. Chem. Engng. 67 (1989) 361–367.
[28] J.N. Lin, F.C. Chou, P.Y. Tzeng, Theoretical prediction of the onset of thermal instability in the thermal entrance region of horizontal rectangular channels, Int. J. Heat Fluid Flow 12 (1991) 218–224.
[29] T.S. Lee, P.G. Parikh, A. Acrivos, D. Bershader, Natural convection in a vertical channel with opposing buoyancy forces, Int. J. Heat Mass Transfer 25 (1982) 499–511.
[30] W.M. Yan, Y.L. Tsay, T.F. Lin, Simultaneous heat and mass transfer in laminar mixed convection flows between vertical parallel plates with asymmetric heating, Int. J. Heat Fluid Flow 10 (1989) 262–269.
[31] R.W. Lyczkowski, C.W. Solbrig, D. Gidaspow, Forced convection heat transfer in rectangular ducts – general case of wall resistance and peripheral conduction for ventilation cooling of nuclear waste repositories, Nucl. Engng. Design 67 (3) (1981) 357–378.
[32] R.K. Shah, A.L. London, Laminar Flow Forced Convection in Ducts, Advances in Heat Transfer, Academic Press, New York, 1978 [Chapter VII].
[33] I. Demirzic, M. Peric, Finite volume method for prediction of fluid flow in arbitrarily shaped domains with moving boundaries, Int. J. Numer. Meth. Fluids 10 (1990) 771–790.